Anurova, Irina; Carlson, Synnöve; Rauschecker, Josef P

Overlapping Anatomical Networks Convey Cross-Modal Suppression in the Sighted and Coactivation of "Visual" and Auditory Cortex in the Blind

Published in:
Cerebral Cortex

DOI:
10.1093/cercor/bhz021

Published: 01/03/2019

Document Version
Peer reviewed version

Please cite the original version:
Anurova, I., Carlson, S., & Rauschecker, J. P. (2019). Overlapping Anatomical Networks Convey Cross-Modal Suppression in the Sighted and Coactivation of "Visual" and Auditory Cortex in the Blind. *Cerebral Cortex*, [bhz021]. https://doi.org/10.1093/cercor/bhz021

Overlapping anatomical networks convey cross-modal suppression in the sighted and co-activation of "visual" and auditory cortex in the blind

Irina Anurova [1,2], Synnöve Carlson [3,4], Josef P. Rauschecker [2,5]

[1] Helsinki Institute of Life Science, Neuroscience Center, University of Helsinki, Helsinki, 00014 Finland

[2] Department of Neuroscience, Georgetown University Medical Center, Washington, DC 20057 USA

[3] Department of Neuroscience and Biomedical Engineering, School of Science, Aalto University, Espoo, 02150 Finland

[4] Department of Physiology, Faculty of Medicine, University of Helsinki, Helsinki, 00014 Finland

[5] Institute for Advanced Study, Technical University of Munich, Munich, 85748 Germany

Address correspondence to Irina Anurova, Helsinki Institute of Life Science, Neuroscience Center, P.O. Box 21 (Haartmaninkatu 3 B), FI-00014 University of Helsinki, Finland. Email: irina.anurova@helsinki.fi; Josef P. Rauschecker, New Research Building, WP-19, Department of Neuroscience, Georgetown University Medical Center, 3970 Reservoir Rd. NW, Washington, DC 20007, USA. Email: rauschej@georgetown.edu

Abstract

In the present combined DTI/fMRI study we investigated adaptive plasticity of neural networks involved in controlling spatial and non-spatial auditory working memory in the early blind (EB). In both EB and sighted controls (SC), fractional anisotropy (FA) within the right inferior longitudinal fasciculus correlated positively with accuracy in a one-back sound localization but not sound identification task. The neural tracts passing through the cluster of significant correlation connected auditory and "visual" areas in the right hemisphere. Activity in these areas during both sound localization and identification correlated with FA within the anterior corpus callosum, anterior thalamic radiation, and inferior fronto-occipital fasciculus. In EB, FA in these structures correlated positively with activity in both auditory and "visual" areas, whereas FA in SC correlated positively with activity in auditory and negatively with activity in visual areas. The results indicate that frontal white matter conveys cross-modal suppression of occipital areas in SC, while it mediates co-activation of auditory and reorganized "visual" cortex in EB.

Keywords: blindness; cross-modal plasticity; auditory working memory; functional magnetic resonance imaging (fMRI); diffusion tensor imaging (DTI)

Introduction

Evidence of functional reorganization of deprived sensory cortices in humans has accumulated rapidly during the last two decades. Furthermore, morphometric studies have provided evidence of structural alterations caused by long-term vision loss in deprived sensory brain areas and beyond. These changes include white-matter atrophy in the afferent pathways to the striate cortex, reduced thalamic and occipital grey matter (Noppeney et al. 2005; Pan et al. 2007; Ptito et al. 2008; Bridge et al. 2009; Lepore et al. 2010) along with a decreased "visual" cortical surface area (Park et al., 2009), and increased occipital cortical thickness (Bridge et al. 2009; Jiang et al. 2009; Park et al. 2009; Voss and Zatorre 2012; Anurova et al. 2015).

Development of diffusion tensor imaging (DTI) opened new perspectives for neural plasticity research. Most typical white-matter alterations observed in DTI studies in blind individuals consist of decreased fractional anisotropy (FA) and increased mean diffusivity (MD) within the visual pathways, including the optic nerve (Zhang et al. 2012), optic tract (Park et al. 2007), optic radiation (Shimony et al. 2006; Park et al. 2007; Yu et al. 2007; Shu et al. 2009a; Wang et al. 2013; Lee et al. 2014; Dietrich et al. 2015; Lao et al. 2015; Aguirre et al. 2016; Reislev et al. 2016a), as well as commissural fibers connecting visual cortices and passing through the splenium of the corpus callosum (Shimony et al. 2006; Park et al. 2007; Yu et al. 2007; Wang et al. 2013; Lao et al. 2015; Aguirre et al. 2016; Reislev et al. 2016a). In addition, reduced white-matter integrity has been reported for long association fibers connecting occipital areas with the temporal and frontal lobes (Bridge et al. 2009; Shu et al. 2009b; Lee et al. 2014; Dietrich et al. 2015; Reislev et al. 2016a, 2016b). Furthermore, it is noteworthy that no new neural pathways have been found in either late or early blind individuals, and the vast majority of studies reported no strengthened connectivity within existing pathways.

Functional connectivity studies provided further information about reorganization of large-scale brain networks in blind individuals. In accordance with the above structural connectivity studies, reduced resting-state functional connectivity is often observed between the deprived visual cortex and sensory areas of the intact modalities in blind individuals (Liu et al. 2007; Yu et al. 2008; Bedny et al. 2011; Butt et al. 2013; Burton et al. 2014; Heine et al. 2015; Striem-Amit et al. 2015). On the other hand, in studies that employed an auditory or somatosensory cognitive task, functional connectivity between the deprived visual cortex and sensory cortices of task-relevant modalities was increased (Stilla et al. 2008; Klinge et al. 2010; Sani et al. 2010; Dormal et al. 2016; Pelland et al. 2017). The latter observation is consistent with the results of numerous functional neuroimaging studies, in which concomitant activation of the occipital cortex and sensory cortices of task-relevant modalities was documented in blind individuals (Renier et al. 2010; Collignon et al. 2011; Collignon et al. 2013; Dormal et al. 2016). In sighted individuals, by contrast, visual areas show cross-modal deactivation in tasks requiring attention to stimuli of other sensory modalities (Kawashima et al. 1999; Laurienti et al. 2002; Shomstein and Yantis 2004; Johnson and Zatorre 2005, 2006; Ciaramitaro et al. 2007; Mozolic et al. 2008; Renier et al. 2010). It has earlier been suggested that co-activation of the occipital cortex in various non-visual tasks is supplied by indirect connections between the "visual" and other sensory cortices via higher-order association structures (Fujii et al. 2009; Sani et al. 2010), although direct connections may contribute to activation of the "visual" cortex of blind individuals by non-visual information as well (Klinge et al., 2010). White-matter integrity of the superior longitudinal fasciculus (SLF) was found to predict both accuracy of a visual working memory task performance and BOLD responsivity within the fronto-parietal network in sighted individuals (Burzynska et al. 2011). Weeks et al. (2000) reported that, during an auditory localization task, activity in the posterior parietal cortex of congenitally blind individuals correlated positively with activity in occipital "visual" areas, whereas this correlation was negative in

sighted controls, demonstrating that, in the blind, the occipital areas had become part of a functional network in auditory localization. Thus, the top-down modulation of "visual" cortex activity in both sighted and blind individuals is likely accomplished through anatomical pathways connecting sensory areas with fronto-parietal regions exerting a gating function.

The present study was designed to test the hypothesis that among early blind (EB) individuals, stronger anatomical connections between sensory and higher-order association areas underlie more efficient co-activation of the auditory and deprived visual areas during auditory task performance. Moreover, the same anatomical pathways may be expected to play a role in reciprocal relationships between auditory and visual cortices in sighted individuals.

Furthermore, we hypothesized that the stronger anatomical connectivity may be associated with better behavioral performance. In an earlier study (Renier et al. 2010), accuracy in the auditory localization task in the EB correlated positively with activation in the right middle occipital gyrus (MOG), which is known to be involved in the processing of visual spatial information in the sighted. Thus, we hypothesized that accuracy in an auditory spatial task depends on white-matter microstructure within neural pathways connecting the right-hemispheric MOG with other structures involved in auditory spatial processing.

To test our predictions, we performed a study combining functional magnetic resonance imaging (fMRI) and DTI in EB and sighted individuals. The DTI measures FA, MD, axial and radial diffusivity (AD and RD, respectively) across the whole-brain white-matter skeleton were correlated with the amplitude of activation in the auditory and "visual" regions during performance of spatial and nonspatial auditory tasks. To our knowledge, this is the first attempt to study how the relationship between the brain's structural connectivity and functional activation of cortical areas depends on early visual experience.

Materials and Methods

Participants

Diffusion tensor imaging (DTI) and functional neuroimaging data were obtained from 15 early blind (EB) (5 males, mean age ± standard deviation (S.D.): 52 ± 9.4 years) and 15 sighted control (SC) volunteers (7 males, mean age ± S.D.: 41 ± 11.3 years), which served as controls. All participants were healthy, with no history of neurological or psychiatric disorders. Twelve of the blind participants were blind from birth and 3 became blind by the second year of life. Six blind participants reported some light sensitivity with no form perception. Clinical characteristics of the blind subjects are presented in Table 1. The study protocol was approved by Georgetown University's Institutional Review Board. Written informed consent was obtained from all participants prior to the experiment.

Experimental Design

Subjects performed auditory identification (ID) and localization (LOC) one-back tasks. The stimuli (duration 1000 ms including 10 ms rise/fall times, interstimulus interval 1000 ms) were 4 C-major piano chords over a range of 4 octaves originating from 4 different locations in virtual auditory space. The stimuli were presented via electrostatic MRI-compatible headphones (STAX). Four sound source locations, ±90° (corresponding to the extreme left and right) and ±30°, were simulated by convolving the stimuli with standard head-related transfer functions provided by Amphiotik Synthesis. Subjects were instructed to compare each new stimulus in the sequence with the previous one and categorize it as either the same or different regarding a certain stimulus attribute. During the ID task, subjects compared the chords in terms of pitch height, while in the LOC task they compared the chords' spatial locations. In matching trials, subjects pressed the left button of the MRI-compatible response pad with the left middle finger; in nonmatching trials, they pressed the right button with the left index finger. In the ID task, the spatial location of the sounds was fixed within one block,

but varied among blocks. Conversely, in the LOC task, the same chord was presented from different locations, whereas the chord's height was fixed during one block and varied from one block to another. The onset of each task was announced through the headphones. Presentation of the stimuli and collection of behavioral data were controlled by Superlab software 4.0 (Cedrus Corp.). Sighted subjects were blindfolded during the scanning session. Acquisition of functional data was performed using a block-design paradigm. Blocks (duration 18 s) were separated by 12-s resting periods. Each task was repeated 6 times during one run; three runs were presented during the experiment. The order of the experimental tasks was counterbalanced across subjects.

Statistical Evaluation of Behavioral Data

Analysis of behavioral data (percent correct responses) was performed with a two-way mixed-design ANOVA with Group (EB vs. SC) as a between-subjects factor and Task (ID vs. LOC) as a within-subject factor.

Neuroimaging Data Acquisition

All neuroimaging data were acquired at Georgetown University's Center for Functional and Molecular Imaging on a 3-Tesla Siemens Tim Trio scanner equipped with a 12-channel head coil. The DTI data were collected in the same imaging session as the fMRI data reported in Renier et al. (2010) and have not been published previously. The auditory fMRI data were reanalyzed for this study and data from six participants were added (3 EB and 3 SC).

A high-resolution 3D T1-weighted MPRAGE image (resolution $1 \times 1 \times 1$ mm^3) was acquired for each subject (TR = 1900 ms, TE = 2.52 ms, TI = 900 ms, flip angle = 9°). The volume consisted of 176 sagittal slices (FOV = 256×256 mm^2, 256×256 matrix, slice thickness = 1 mm).

The DTI data were acquired using an echo-planar imaging (EPI) sequence at the end of an experimental session. The integral parallel acquisition technique (iPAT) was used with an acceleration factor of 2 in order to reduce image distortion from susceptibility artifacts. The diffusion sensitizing gradients were applied along 30 non-collinear directions (b = 1000 s/mm^2). The DTI data set also included five non-diffusion-weighted images (b = 0 s/mm^2). For each volume, 55 axial slices were acquired in an interleaved order (slice thickness = 2.5 mm, spacing between slices = 2.5 mm) using TR = 6300 ms and TE = 86 ms. The FOV was 192 × 192 mm^2 with a 96 × 96 matrix size. In order to improve the signal-to-noise ratio, the acquisitions were repeated twice.

The fMRI data were acquired using an echo-planar imaging sequence (flip angle = 90°, TR = 3 s, TE = 60 ms). The FOV was 192 × 192 mm^2 with a 64 × 64 matrix size; slice thickness was 2.8 mm with a 0.2-mm gap, resulting in an effective voxel resolution of 3 × 3 × 3 mm^3. For each run, 184 volumes of 50 slices were acquired in a continuous sampling paradigm with auditory stimulus amplitudes well above the background of the scanner noise (Renier et al., 2010; Anurova et al., 2015).

Neuroimaging Data Processing and Analysis

DTI

DTI data preprocessing and analysis were performed with FMRIB's software library (FSL, version 5.0, Oxford Centre for Functional MRI of the Brain (FMRIB), UK: http://www.fmrib.ox.ac.uk/fsl/) using a standard processing pipeline. First, image distortions caused by eddy currents and small head movements were minimized by affine registration of each individual diffusion-weighted image to the subject's b0 image. The Brain Extraction Tool (BET) (Smith 2002) was applied for extracting brains from the b0 images and creating the individual brain masks. The brain masks were then applied for all volumes within the 4D data sets. After that, the DTI model was fitted voxel-wise using the DTIFIT algorithm

resulting in calculating the 3D maps for axial (1st) and transverse (2nd and 3rd) eigenvectors and eigenvalues, FA and MD. Between-group comparisons of the DTI measures such as FA, MD, AD and RD as well as testing correlations of the DTI measures with behavioral and functional data were performed using the Tract-Based Spatial Statistics (TBSS) (Smith et al. 2006), part of FSL (Smith et al. 2004). Each individual FA image was aligned to every other one using the nonlinear registration tool FNIRT (Andersson et al. 2007a, 2007b), and the "most representative" subject in the study was automatically identified as a target. This target image was then affine-transformed into MNI152 standard space. After that, each individual FA images were transformed into 1x1x1 mm3 MNI152 space by combining the nonlinear transform to the target with the affine transform from the target to MNI152 space. Then, a mean of all 30 transformed FA images was calculated and thinned to create a mean FA skeleton which represented the centers of all tracts common to the group. The skeleton was thresholded at FA = 0.2. Next, each subject's aligned FA data were projected onto this skeleton by filling the skeleton with FA values from the nearest relevant tract center. This was done, for each skeleton voxel, by selecting the maximum FA value in the subject's aligned image from a subset of voxels perpendicular to the local skeleton structure. Finally, the resulting data were fed into voxel-wise cross-subject statistics. The skeletonized data sets were also created for the AD ($\lambda1$), RD (($\lambda2+\lambda3$)/2) and MD (($\lambda1+\lambda2+\lambda3$)/3) measures using the tbss_non_FA script.

Voxel-wise statistics on the skeletonised data were carried out using the Randomise tool (part of FSL) for nonparametric permutation inference on neuroimaging data with 5000 permutations. First, we looked for group differences in all DTI measures (FA, AD, RD and MD) using a general linear model (GLM), controlling for age and gender. The significance threshold for all statistical tests was set at $P < 0.05$ after correcting for family-wise error using the threshold-free cluster enhancement (TFCE). Next, we studied the relationship between the behavioral data (accuracy of the ID and LOC task performances) and each DTI measure. The

GLMs also included age and gender as covariates. The models tested both main effects (Performance accuracy) and Group x Performance accuracy interactions. If significant correlations between the behavioral and DTI measures or interactions between them were observed, probabilistic fiber tracking was performed in order to determine the brain areas that were interconnected by the neural tracts passing through the significant cluster. Prior to fiber tracking, distributions of diffusion parameters at each voxel were calculated using the BEDPOSTX tool (part of FSL) (Behrens et al. 2003; Behrens et al. 2007). At this step, probabilistic tractography with PROBTRACKX tool (part of FSL) (Behrens et al. 2003; Behrens et al. 2007) was carried out using a significant cluster as a seed. Number of permutations was 5000. The resulting fibers were normalized by dividing the paths by the number of seed voxels multiplied by the number of permutations and multiplying the result by 100%, and then averaged across each group of subjects.

fMRI

The fMRI data were used for localization of functional regions of interest (ROI) within auditory and "visual" cortical areas.

Analysis of fMRI data was performed in surface space using Brain Voyager 2.1 (BVQX, Brain Innovation, Maastricht, Netherlands). An intersubject cortical alignment procedure was employed in order to reduce the effect of anatomical variability and to improve the spatial correspondence of cortical areas between individual brains. Prior to the surface reconstruction, the original T1-weighted MRIs were corrected for spatial intensity inhomogeneity and then spatially transformed into standard Talairach space (Talairach and Tournoux 1988) using sinc interpolation. Then the volumes were automatically segmented to white (WM) and gray (GM) matter. Topological errors such as "bridges" and remaining fragments of dura mater or cerebellum were corrected manually. The reconstructed cortical hemispheres were morphed into spherical representations of the folded cortex. Curvature

information of 30 individual brains (15 EB and 15 SC) was used for cortex-based intersubject alignment, which was carried out using the moving-target group averaging (Goebel et al. 2006) and resulted in creating averaged curvature maps. After the alignment procedure, averaged folded meshes were constructed for both hemispheres for projecting the fMRI data.

The preprocessing of the functional data included slice-timing correction, correction for small interscan head movements, temporal high-pass filtering (removing frequencies lower than 3 cycles/run), and spatial smoothing using a 6-mm Gaussian filter and transformation into Talairach space. A general linear model (GLM) was used to analyze the blood oxygen level–dependent (BOLD) responses of each subject as a function of experimental condition. Regressors of interest consisted of boxcar functions convolved with the standard hemodynamic response function. A random-effects analysis of variance (RFX ANOVA) was employed in order to remove intersubject variability. The RFX ANOVA was applied in cortical surface space following the cortical reconstruction and intersubject alignment.

The whole-brain analysis was carried out using two contrasts: EB (ID+LOC) + SC (ID+LOC) and EB (ID+LOC) – SC (ID+LOC), in order to define functional ROIs within temporal and occipital cortical areas. The first contrast was used to define ROIs involved during auditory one-back task performance in both groups (presumed to be in auditory cortex), while the second contrast was employed to define ROIs that show maximum activity differences between the two groups (presumably within occipital cortex). The P values were corrected for false discovery rate (FDR) using a threshold of $q < 0.05$. The whole-brain analysis was carried out using two contrasts: EB (ID+LOC) + SC (ID+LOC) and EB (ID+LOC) – SC (ID+LOC), in order to define functional ROIs within temporal and occipital cortical areas. The first contrast was used to define ROIs involved during auditory one-back task performance in both groups (presumed to be in auditory cortex), while the second contrast was employed to define ROIs that show maximum activity differences between the two

groups (presumably within occipital cortex). The P values were corrected for false discovery rate (FDR) using a threshold of $q < 0.05$. Cortical patches around 10 mm in diameter showing maximal percentage of signal change and located within bilateral CS, LO and STG were defined as ROIs, as shown in Fig. 4 A. The ROI's activity was further correlated with FA, AD, RD and MD across the whole skeleton, in order to identify white-matter structures which may mediate cross-modal suppression of occipital areas in SC and co-activation of auditory and reorganized "visual" cortex in EB.

The mean ROI activity was further correlated with accuracy of task performance. We employed an analysis of partial correlations using subjects' age and gender as controlling variables. The P-values were adjusted using Bonferroni correction. The adjustments were done separately for each ROI in both groups.

Studying relationships between fMRI and DTI data

The mean ROI activity during ID and LOC task performances (versus baseline) was submitted as a continuous variable to the GLM, which also included age and gender as covariates and Group as a categorical variable. We examined both the main effect of ROI activation and Group x ROI activation interaction. If a significant main effect or interaction was found, probabilistic fiber tracking was performed, in order to identify neural pathways involved in controlling the ROI's activity. Tractography was performed similarly as described above, using a significant cluster identified within the FA skeleton as a seed. The resulting fiber tracts were normalized and averaged across each group of subjects.

In addition, we performed an analysis of partial correlations between each ROI's mean activity and the mean FA/diffusivity within the resulting significant cluster. Subjects' age and gender were used as controlling variables. The analysis was done in order to test whether the correlations between the percentage of signal change and FA/diffusivity values had the same or opposite directions in the groups of EB and SC subjects.

Results

Behavioral Data

The accuracy of one-back identification (ID) and localization (LOC) task performances did not differ between groups ($F(1,28) = 3.06$, $P = 0.09$) or experimental tasks ($F(1,28) = 0.38$, $P = 0.54$). Both EB subjects and sighted controls (SC) managed auditory ID and LOC tasks at high, but not at ceiling accuracy levels (EB, 85 ± 3% (mean ± standard error of mean) for the ID task and 83 ± 3% for the LOC task; SC, 90 ± 2% and 91 ± 2%, respectively).

TBSS analysis of the DTI data

Fractional anisotropy was significantly reduced in the group of EB compared to SC in extensive white-matter regions within the bilateral geniculo-calcarine tracts (GCT), also known as optic radiations, the bilateral inferior longitudinal fasciculi (ILF), and the posterior part (isthmus and splenium) of the corpus callosum (pCC). Decreased FA was also found in the anterior part (genu) of the corpus callosum (aCC) and bilaterally in the anterior part of the external/extreme capsule, which includes the inferior fronto-occipital (IFOF) and uncinate (Unc) fasciculi. Other clusters of reduced FA were located within the corticospinal tract (CST), and in the anterior limb of the internal capsule (ALIC), which includes the anterior thalamic radiation (ATR) and the fronto-pontine tract (Fig. 1 A).

Axial diffusivity was significantly increased in the group of EB compared to SC in two small left-hemispheric clusters which belonged to the CST and IFOF (Fig. 1 B).

Significant increases in RD in the group of EB compared to SC were observed in white-matter regions which largely overlapped with those of significant FA decreases. Increased RD was found bilaterally within the GCT and ILF, in the anterior and posterior parts of the CC, and bilaterally in the anterior part of the external capsule, CST, and in the anterior limb of the internal capsule (Fig. 2 A).

Mean diffusivity (MD) was also increased in the group of EB compared to SC. The regions of MD increases were almost identical to the regions of RD increases, although they were less extensive and more lateralized to the left hemisphere. Significant clusters were located within the bilateral GCT, bilateral ILF, pCC, aCC, left external capsule and left anterior limb of the internal capsule. In addition, MD increases were observed bilaterally within the posterior limb of the external capsule, which includes the CST and the ascending medial and lateral lemnisci (Fig. 2 B).

Correlations between behavioral and DTI data

Analysis of the relationship between behavioral and skeletonized DTI data showed that the accuracy of the LOC task performance correlated positively with FA within the right-hemispheric ILF (Fig. 3 A). Although the mean FA values within the resulting cluster were significantly lower in the group of EB ($t(28) = 2.26$, $p < 0.05$), confirming the results of the whole-skeleton TBSS analysis, positive correlations between sound localization accuracy and FA were significant in both groups (in EB: $r_p = 0.88$, $p < 0.001$; in SC: $r_p = 0.73$, $p < 0.01$). Higher FA values were associated with better performance (Fig. 3 B). No significant correlations were found between the FA and performance accuracy during the ID task.

Other measures of diffusivity (AD, RD and MD) did not correlate with performance accuracy in either of the tasks.

Probabilistic tractography using the significant FA cluster (Fig. 3 A) as a seed showed that the cluster belonged to the superior branch of the right-hemispheric ILF that connects auditory cortex in the superior temporal gyrus (STG) with primary (calcarine sulcus, CS) and non-primary (lateral occipital, LO) "visual" areas (Fig. 3 C and D).

Defining functional ROIs

Functional ROIs were defined within bilateral occipital and temporal cortices that were functionally relevant for the performance of the experimental tasks.

In the present study, the mean ROI activity was used as a predictor in the GLM applied to the skeletonized FA data, in order to identify grey- and white-matter components of a neural network involved in auditory working memory processing in EB and SC. We performed the same analysis for both tasks to look for potential differences in subcomponents of the network controlling auditory spatial and non-spatial processing. The contrast EB (ID+LOC) – SC (ID+LOC) allowed to identify occipital areas showing significant differences in activation between the two groups of participants. The resulting ROIs were approximately 10 mm in diameter around the local maximum. The center Talairach coordinates of the resulting ROIs were located in CS (left hemisphere: x = –9, y = –88, z = 0; right hemisphere: x = 8, y = –86, z = 1) and LO (left hemisphere: x = –36, y = –78, z = 2; right hemisphere: x = 43, y = –70, z = –1). The STG ROIs (left hemisphere: x = –56, y = –22, z = 7; right hemisphere: x = 55, y = –19, z = 9) was identified using the contrast EB (ID+LOC) + SC (ID+LOC).

Correlations between behavioral and fMRI data

In the group of EB, the mean activity within the right LO ROI correlated positively with behavioral accuracy during the LOC task performance (r_p = 0.69, $p < 0.05$, Bonferroni-corrected). In SC, in contrast, the mean activity within the right LO ROI correlated negatively with behavioral accuracy during the ID task performance (r_p = –0.70, $p < 0.05$, Bonferroni-corrected).

Correlation between functional and DTI data

The mean activity in the right STG ROI during ID task performance correlated positively with FA in several prefrontal white-matter structures, which included the aCC/Forceps Minor and the intersection of the left internal and external/extreme capsules (Fig. 4 B).

In order to distinguish the tracts passing through a particular cluster in which significant correlations between FA and fMRI activity were observed, probabilistic fiber tracking was performed using that cluster as a seed. The tractography results showed that the voxels of the cluster belonged to bilateral ATR, left IFOF and transcallosal pathways connecting the left and right inferior, middle and medial frontal areas (Fig. 4 D).

The mean FA within the cluster was reduced in EB compared to SC ($t(28) = 2.58$, $p < 0.05$), however, positive correlations between the STG activation and FA were significant in both groups (in EB: $r_p = 0.77$, $p < 0.01$; in SC: $r_p = 0.73$, $p < 0.01$). Higher FA values were associated with stronger STG activation during ID task performance (Fig. 4 C).

Significant positive correlation between FA and activity of the right STG ROI during the LOC task performance was observed within more extended white-matter areas, compared to the ID task, which included prefrontal (aCC/Forceps Minor, anterior limb of the left internal capsule and the intersection of the left internal and external/extreme capsules) and parietal structures (Fig. 5 A). Probabilistic tractography, using the cluster in which correlation between FA and STG activation was significant, as a seed, showed that frontal voxels belonged to bilateral ATR, left IFOF and transcallosal pathways connecting the left and right inferior, middle, superior and medial frontal areas. Parietal voxels belonged to the SLF, which is part of the auditory dorsal pathway (Rauschecker and Tian 2000; Tian et al. 2001) (Fig. 5 C).

The mean FA within the cluster was also reduced in EB compared to SC ($t(28) = 2.56$, $p < 0.05$), and positive correlations between the STG activation during LOC task performance and FA were significant in both groups (in EB: $r_p = 0.85$, $p < 0.001$; in SC: $r_p = 0.76$, $p < 0.01$). (Fig. 5 B).

For both occipital ROIs (CS and LO), significant interactions between Group and ROI activation were observed. Activity of the right CS ROI during ID task performance correlated

with FA values positively in the group of EB (r_p = 0.79, $p < 0.001$) and negatively in the group of SC (r_p = –0.96, $p < 0.001$) (Fig. 6 B). White-matter voxels exhibiting significant statistical effect were located within Forceps Minor and the intersections of the internal and external/extreme capsules in both hemispheres (Fig. 6 A). Probabilistic tractography from the cluster of significant Group x Activation interaction showed that the voxels of the cluster belonged to bilateral ATR, bilateral IFOF and transcallosal pathways connecting left and right inferior, middle and medial frontal areas (Fig. 6 C). The mean FA within the cluster was reduced in EB compared to SC ($t(28) = 2.19$, $p < 0.05$).

Activity of the right LO ROI during LOC task performance correlated positively with FA values in the group of EB (r_p = 0.63, $p < 0.05$) and negatively in the group of SC (r_p = –0.75, $p < 0.01$) within an extended frontal cluster (Fig. 6 E). Voxels with significant correlations were located within the anterior and middle parts of the corpus callosum and the intersections of the internal and external/extreme capsules in both hemispheres (Fig. 6 D). Tractography results showed that significant voxels belonged to bilateral ATR, left IFOF and transcallosal pathways connecting the left and right inferior, middle, superior and medial frontal areas (Fig. 6 F). The mean FA within the cluster was also reduced in EB compared to SC ($t(28) = 3.00$, $p < 0.01$).

In the left hemisphere, activity within the STG during LOC task performance correlated with FA values within the aCC/Forceps Minor and the intersection of the left internal and external/extreme capsules (Fig. 5 D). In both groups correlations were positive: r_p = 0.93, $p < 0.001$ for EB and r_p = 0.65, $p < 0.05$ for SC (Fig. 5 E). The mean FA within the cluster was reduced in EB compared to SC ($t(28) = 2.36$, $p < 0.05$). Tractography results showed that significant voxels belonged to bilateral ATR, left IFOF and transcallosal pathways connecting the left and right inferior, middle, superior and medial frontal areas (Fig. 5 F). No other significant effects or interactions for the left-hemispheric ROIs were found.

Other measures of diffusivity (AD, RD and MD) did not correlate with the mean ROI activity in either of the tasks.

Discussion

We investigated relationships between white-matter microstructure and functional activation as well as performance accuracy, during auditory spatial and nonspatial tasks in EB and SC. Besides group differences in white-matter diffusion properties, we found significant correlations between structure and function. The FA within the right ILF correlated positively with accuracy of one-back sound LOC task performance in both groups of participants. Probabilistic fiber tracking identified a tract connecting right-hemispheric auditory cortex with lateral and medial occipital areas as the structural basis for this relationship. Moreover, activity in superior temporal and occipital areas correlated with FA in several frontal white-matter structures. For the temporal cortex, correlations were positive in both EB and SC, whereas for the occipital regions, correlations were positive in EB and negative in SC. Importantly, the level of activity within right-hemispheric occipital cortex correlated with performance accuracy in both groups: stronger activation of the LO area in EB and stronger deactivation of the same area in SC was associated with more accurate performance of the auditory tasks and hence with more efficient top-down control.

Group differences in white-matter diffusion properties between EB and SC

We found group differences in all diffusion parameters, particularly in FA and RD, throughout the occipital lobes and beyond. FA was decreased, while all diffusivity measures were increased in EB compared to SC.

FA, which reflects several microstructural features such as fiber density and coherence as well as myelin content of the tissue (Beaulieu 2002; Le Bihan 2006; Schmierer et al. 2007; Feldman et al. 2010; Kolasinski et al. 2012), was reduced in EB in widespread white-matter

regions including the occipital lobes. Conversely, RD, which is highly sensitive to the degree of axonal myelination, axonal diameter and density of axonal packing (Song et al. 2002; Song et al. 2005; Mori and Zhang 2006; Alexander et al. 2007; Sun et al. 2008; Feldman et al. 2010; Onu et al. 2012), was increased in EB in white-matter regions largely overlapping with regions where FA reductions were detected. The most prominent differences were found in tracts associated with visual functions: the geniculo-calcarine tracts, ILF, and the splenium of the corpus callosum. This result is in line with previous observations in early and late blind individuals (Shimony et al. 2006; Park et al. 2007; Yu et al. 2007; Bridge et al. 2009; Shu et al. 2009a; Wang et al. 2013; Lee et al. 2014; Aguirre et al. 2016; Reislev et al. 2016a; Reislev et al. 2016b).

Furthermore, in accord with earlier findings (Wang et al. 2013; Dietrich et al. 2015), decreased FA and increased RD were observed within the ATR, which connects the anterior and midline thalamic nuclei with the frontal lobe and is strongly associated with cognitive functions such as working memory and executive control (Mamah et al. 2010). Thalamic interneurons of the medial dorsal nucleus (MDN) process information from different sensory modalities and exchange this information with dorsolateral and ventrolateral prefrontal cortical areas. Therefore, the observed FA reduction within the ALIC may be partially due to reduced input from the LGN to the MDN. Another explanation for the altered microstructure of the ALIC in EB may be a general reduction of motor activity of blind individuals (Brambring 2001), since the fronto-pontine tract is involved in the coordination of planned motor functions (Rea 2015).

Neuronal mechanisms underlying white-matter structural alterations in the blind

Accumulating evidence suggests that myelination is sensitive to neuronal activity. In the normally developing brain, oligodendrocytes preferentially myelinate electrically active axons (Demerens et al. 1996; Stevens et al. 2002; Fields 2004; Ishibashi et al. 2006; Gautier et al.

2015; Wake et al. 2015). As a result of its dependency on neuronal activity, myelination appears to be sensitive to environmental constraints. For example, loss of neuronal activity due to sensory deprivation may lower the survival of newly divided progenitor cells and result in a significant decrease in white-matter integrity (Hill et al. 2014; Dietz et al. 2016). Using animal models has allowed discovering specific microstructural changes in response to prolonged sensory deprivation. Unilateral trimming of the facial vibrissae in mice causes a significant decrease in myelinated axons in the barrel cortex and reduces the amount of myelin ensheathing each axon (Barrera et al. 2013). Furthermore, long-term monocular deprivation in mice has been shown to shorten myelin internode lengths (Etxeberria et al. 2016). These microstructural alterations are associated with reductions in both velocity and fidelity of action potential transmission. Coordinating conduction time between different cortical and subcortical regions is essential for the summation of convergent inputs and thus for the accomplishment of higher-level cognitive functions (Fields 2004). As a consequence, compensatory alterations in white-matter properties causing a reduction in conduction velocity may spread beyond the visual system.

Relationship between brain structure, function and behavior

Perhaps the most significant finding of the present study was the positive correlation of FA within the superior branch of the right ILF with accuracy in a one-back sound LOC task in both groups of participants. This pathway connects the auditory cortex in the right STG with lateral and medial occipital areas (Fig. 3 C, D). Specifically, the right hemisphere has been implicated in spatial processing (Baumgart et al. 1999; Weeks et al. 2000; Zatorre and Penhune 2001; Spierer et al. 2009; Weisz et al. 2014). Furthermore, activity of the right LO region in the present study correlated with frontal white-matter FA during the LOC but not the ID task. The center coordinates of this region were similar to those of the human middle temporal area (Watson et al. 1993; Dumoulin et al. 2000) and the right MOG area, which was

shown to be preferentially involved in both auditory and tactile localization in EB (Renier et al. 2010). In both groups of participants, fibers passing through white-matter clusters with significant correlation between FA and ROI activity during the ID task mostly connected with inferior frontal areas (Figs. 4 D and 6 C), whereas fibers passing through clusters identified during the LOC task connected with both inferior and superior frontal and parietal areas (Figs. 5 C, F; 7 C).

The caudal (posterior-dorsal) part of nonprimary auditory cortex in rhesus monkeys has been shown to support functions of auditory spatial processing (Rauschecker and Tian 2000; Recanzone 2000). Injection of anatomical tracers into its caudolateral area leads to labeling of dorsolateral prefrontal cortex, thus defining an anatomical dorsal pathway for auditory spatial processing that projects from posterior STG to parietal and frontal areas (Romanski et al. 1999). Human studies show a similar segregation between spatial and nonspatial auditory processing at the level of nonprimary auditory cortex: posterior parts of the supratemporal plane (planum temporale, PT) are associated with processing sound location, and anterior parts with processing spectral characteristics and sound identity (Warren and Griffiths 2003; Ahveninen et al. 2006; Barrett and Hall 2006). While it seems clear that the dorsal pathway corresponds to the SLF, the correspondence between the auditory ventral pathway and the ILF is less obvious, especially given the lack of information about directionality of fibers in DTI studies (e.g. Schmahmann et al. 2007; Saur et al. 2008; Mars et al. 2016). The ILF may consist of fibers projecting anteriorly to ventrolateral prefrontal cortex as part of the ventral stream, while other fibers feed from the PT into the dorsal stream for spatial processing. Comparative studies in humans and monkeys with identical neuroimaging techniques will be needed to clarify the organization of ventral and dorsal pathways in both species (Takemura et al. 2017).

In EB, superior temporal and occipital areas are known to be conjointly involved in auditory working memory processing (Renier et al. 2010; Collignon et al. 2011). In SC, however, cross-modal deactivation of occipital areas may be observed (Laurienti et al. 2002; Johnson and Zatorre 2005; Azulay et al., 2009; Anurova et al. 2015). Thus, integrity of the neural tracts connecting auditory and visual areas is important for supplying effective communication between these structures in both groups. However, the identity of the neural connections that mediate such communication remains unknown. Several lines of evidence suggest that even early visual areas are not strictly unimodal and may have a potential for multimodal processing (Murray et al. 2016). For example, neuroanatomical studies in animals (Falchier et al. 2002; Rockland and Ojima 2003) and diffusion-based imaging studies in humans (Beer et al. 2011) have provided evidence of direct connections between primary visual and auditory areas, but their functional significance is still unclear. The present study clearly demonstrates that the integrity of the ILF connecting auditory and visual areas is important for efficiency of behavioral performance, although the amplitude of activation/deactivation of auditory and visual areas did not correlate with FA values within the ILF. Our primary hypothesis was that activity within the auditory and visual cortex is mediated through connections from multisensory cortical and subcortical areas providing efficient co-activation of the auditory and deprived visual areas by an auditory working memory task in EB and reciprocal relationships between auditory and visual cortices in sighted individuals. The GLM analysis employed at the whole-skeleton level revealed that activity in the temporal and occipital areas did indeed correlate with FA within several frontal white-matter structures, such as the anterior part (genu) of the corpus callosum, anterior thalamic radiation and inferior fronto-occipital fasciculus. In the group of EB, FA correlated positively with activity of auditory and "visual" areas, whereas in SC, FA correlated positively with the task-related activity of auditory areas and negatively with activity of "visual" areas. The pattern of correlations between the FA and the auditory and visual cortical

activity suggests a link between the integrity of the neural tract microstructure and strength of activation/deactivation in the related cortical areas and corroborates prior studies on white matter plasticity indicating that experience can shape neural tracts (Lovden et al. 2010; Takeuchi et al. 2010; Mackey et al. 2012; Salminen et al. 2016), e.g., through activity-dependent myelination of axons (Sampaio-Baptista and Johansen-Berg 2017). The fiber tracking results indicate that transcallosal connections between frontal cortices as well as fronto-occipital and fronto-thalamic connections are important for controlling joint activation of auditory and "visual" areas in the blind and reciprocal relationships between these areas in the sighted.

This assumption gains strong support from several neuroimaging studies in children and adults. Increased FA and decreased MD, within the genu of corpus callosum and fornix, has been shown to correlate positively with working memory and problem solving abilities in healthy young adults (Zahr et al. 2009) and elderly individuals (Charlton et al. 2010). Furthermore, increased FA within the genu of corpus callosum and prefrontal white matter was associated with higher processing speed, more efficient verbal and non-verbal working memory and enhanced cognitive flexibility assessed in a task-switching paradigm (Kennedy and Raz 2009). Similarly, in developmental studies, positive correlations between working memory scores and FA values within the genu of the corpus callosum, inferior frontal lobes and SLF were found in 8-18 year-old children (Olesen et al. 2003; Nagy et al. 2004). Moreover, amplitudes of BOLD responses within frontal and parietal regions correlated positively with FA values within the genu of the corpus callosum and the temporo-occipital white matter (Olesen et al. 2003).

Taking into account that in the present study the fibers traced from the clusters of significant correlations always included anterior transcallosal pathways, it appears logical to conclude

that coordinated activity of the left and right frontal cortices plays an essential role in higher-order cognitive functions including but not limited to working memory processing.

Conclusions

White-matter integrity within and beyond occipital lobes depends on visual experience and is, therefore, reduced in early blind individuals. While the most prominent alterations of the white-matter microstructure were observed within neural pathways associated with visual function, additional clusters of reduced FA were found beyond vision-related structures. Despite the significant between-group differences in diffusion properties of the right ILF, FA within this pathway correlated positively with accuracy of behavioral performance in an auditory localization task in both EB and SC individuals. The tract passing through the white-matter cluster of significant correlation between structure and behavior connects the right-hemispheric auditory cortex with lateral and medial "visual" areas. Furthermore, in line with the dual-pathway models of auditory processing (Rauschecker and Tian 2000; Miller and Recanzone 2009), fibers passing through white-matter clusters with significant correlation between FA and STG/CS activity during the ID task, preferentially connect with inferior frontal areas, while fibers passing through the clusters corresponding to the LOC task connect with both inferior and superior frontal and parietal areas. The results of the present study suggest, therefore, that interactions between bilateral frontal cortex and the medial dorsal nucleus of thalamus may be essential for controlling the activity of temporal and occipital areas during auditory working memory processing. While visual areas undergo cross-modal deactivation in sighted individuals, auditory and reorganized visual areas are jointly activated in early blind individuals.

Acknowledgements

This work was supported by grants from the U.S. National Institutes of Health (R01EY018923 and R01DC014989 to J.P.R.), the U.S. National Science Foundation (PIRE-OISE-0730255 to J.P.R.), the Academy of Finland (grant number 123044 to I.A., grant number 259752 to S.C.; a Finland Distinguished Professorship [FiDiPro] award to J.P.R.), and by the Technische Universität München Institute for Advanced Study (TUM-IAS), funded by the German Excellence Initiative and the European Union Seventh Framework Programme under grant agreement no. 291763 (J.P.R.). We wish to thank Dr. Laurent Renier for his help with the design of the fMRI experiment and with neuroimaging data collection.

Author Contributions

Conceptualization, I.A., S.C. and J.P.R.; Methodology, I.A., S.C. and J.P.R.; Investigation, I.A.; Formal Analysis, I.A.; Resources, J.P.R.; Writing – Original Draft, I.A.; Writing – Review & Editing, I.A., S.C. and J.P.R.; Visualization, I.A.; Supervision, S.C. and J.P.R.; Funding Acquisition, I.A., S.C. and J.P.R.

References

Aguirre GK, Datta R, Benson NC, Prasad S, Jacobson SG, Cideciyan AV, Bridge H, Watkins KE, Butt OH, Dain AS, Brandes L, Gennatas ED. 2016. Patterns of Individual Variation in Visual Pathway Structure and Function in the Sighted and Blind. PLoS One. 11:e0164677.

Ahveninen J, Jaaskelainen IP, Raij T, Bonmassar G, Devore S, Hamalainen M, Levanen S, Lin FH, Sams M, Shinn-Cunningham BG, Witzel T, Belliveau JW. 2006. Task-modulated "what" and "where" pathways in human auditory cortex. Proc Natl Acad Sci U S A. 103:14608-14613.

Alexander AL, Lee JE, Lazar M, Field AS. 2007. Diffusion tensor imaging of the brain. Neurotherapeutics. 4:316-329.

Andersson J, Jenkinson M, Smith S. 2007a. Non-linear optimisation. In: FMRIB technical report. p 1-16.

Andersson J, Jenkinson M, Smith S. 2007b. Non-linear registration, aka Spatial normalisation. In: FMRIB technical report. p 1-21.

Anurova I, Renier LA, De Volder AG, Carlson S, Rauschecker JP. 2015. Relationship Between Cortical Thickness and Functional Activation in the Early Blind. Cereb Cortex. 25:2035-2048.

Azulay H, Striem E, Amedi A. 2009. Negative BOLD in sensory cortices during verbal memory: a component in generating internal representations? Brain Topogr. 21:221-231.

Barrera K, Chu P, Abramowitz J, Steger R, Ramos RL, Brumberg JC. 2013. Organization of myelin in the mouse somatosensory barrel cortex and the effects of sensory deprivation. Dev Neurobiol. 73:297-314.

Barrett DJ, Hall DA. 2006. Response preferences for "what" and "where" in human non-primary auditory cortex. Neuroimage. 32:968-977.

Baumgart F, Gaschler-Markefski B, Woldorff MG, Heinze HJ, Scheich H. 1999. A movement-sensitive area in auditory cortex. Nature. 400:724-726.

Beaulieu C. 2002. The basis of anisotropic water diffusion in the nervous system - a technical review. NMR Biomed. 15:435-455.

Bedny M, Pascual-Leone A, Dodell-Feder D, Fedorenko E, Saxe R. 2011. Language processing in the occipital cortex of congenitally blind adults. Proc Natl Acad Sci U S A. 108:4429-4434.

Beer AL, Plank T, Greenlee MW. 2011. Diffusion tensor imaging shows white matter tracts between human auditory and visual cortex. Exp Brain Res. 213:299-308.

Behrens TE, Berg HJ, Jbabdi S, Rushworth MF, Woolrich MW. 2007. Probabilistic diffusion tractography with multiple fibre orientations: What can we gain? Neuroimage. 34:144-155.

Behrens TE, Woolrich MW, Jenkinson M, Johansen-Berg H, Nunes RG, Clare S, Matthews PM, Brady JM, Smith SM. 2003. Characterization and propagation of uncertainty in diffusion-weighted MR imaging. Magn Reson Med. 50:1077-1088.

Brambring M. 2001. Motor activity in children who are blind or partially sighted. Visual Impairment Research. 3:41-51.

Bridge H, Cowey A, Ragge N, Watkins K. 2009. Imaging studies in congenital anophthalmia reveal preservation of brain architecture in 'visual' cortex. Brain. 132:3467-3480.

Burton H, Snyder AZ, Raichle ME. 2014. Resting state functional connectivity in early blind humans. Front Syst Neurosci. 8:51.

Burzynska AZ, Nagel IE, Preuschhof C, Li SC, Lindenberger U, Backman L, Heekeren HR. 2011. Microstructure of frontoparietal connections predicts cortical responsivity and working memory performance. Cereb Cortex. 21:2261-2271.

Butt OH, Benson NC, Datta R, Aguirre GK. 2013. The fine-scale functional correlation of striate cortex in sighted and blind people. J Neurosci. 33:16209-16219.

Charlton RA, Barrick TR, Lawes IN, Markus HS, Morris RG. 2010. White matter pathways associated with working memory in normal aging. Cortex. 46:474-489.

Ciaramitaro VM, Buracas GT, Boynton GM. 2007. Spatial and cross-modal attention alter responses to unattended sensory information in early visual and auditory human cortex. J Neurophysiol. 98:2399-2413.

Collignon O, Dormal G, Albouy G, Vandewalle G, Voss P, Phillips C, Lepore F. 2013. Impact of blindness onset on the functional organization and the connectivity of the occipital cortex. Brain. 136:2769-2783.

Collignon O, Vandewalle G, Voss P, Albouy G, Charbonneau G, Lassonde M, Lepore F. 2011. Functional specialization for auditory-spatial processing in the occipital cortex of congenitally blind humans. Proc Natl Acad Sci U S A. 108:4435-4440.

Demerens C, Stankoff B, Logak M, Anglade P, Allinquant B, Couraud F, Zalc B, Lubetzki C. 1996. Induction of myelination in the central nervous system by electrical activity. Proc Natl Acad Sci U S A. 93:9887-9892.

Dietrich S, Hertrich I, Kumar V, Ackermann H. 2015. Experience-related structural changes of degenerated occipital white matter in late-blind humans - a diffusion tensor imaging study. PLoS One. 10:e0122863.

Dietz KC, Polanco JJ, Pol SU, Sim FJ. 2016. Targeting human oligodendrocyte progenitors for myelin repair. Exp Neurol. 283:489-500.

Dormal G, Rezk M, Yakobov E, Lepore F, Collignon O. 2016. Auditory motion in the sighted and blind: Early visual deprivation triggers a large-scale imbalance between auditory and "visual" brain regions. Neuroimage. 134:630-644.

Dumoulin SO, Bittar RG, Kabani NJ, Baker CL, Jr., Le Goualher G, Bruce Pike G, Evans AC. 2000. A new anatomical landmark for reliable identification of human area V5/MT: a quantitative analysis of sulcal patterning. Cereb Cortex. 10:454-463.

Etxeberria A, Hokanson KC, Dao DQ, Mayoral SR, Mei F, Redmond SA, Ullian EM, Chan JR. 2016. Dynamic Modulation of Myelination in Response to Visual Stimuli Alters Optic Nerve Conduction Velocity. J Neurosci. 36:6937-6948.

Falchier A, Clavagnier S, Barone P, Kennedy H. 2002. Anatomical evidence of multimodal integration in primate striate cortex. J Neurosci. 22:5749-5759.

Feldman HM, Yeatman JD, Lee ES, Barde LH, Gaman-Bean S. 2010. Diffusion tensor imaging: a review for pediatric researchers and clinicians. J Dev Behav Pediatr. 31:346-356.

Fields RD. 2004. Volume transmission in activity-dependent regulation of myelinating glia. Neurochem Int. 45:503-509.

Fujii T, Tanabe HC, Kochiyama T, Sadato N. 2009. An investigation of cross-modal plasticity of effective connectivity in the blind by dynamic causal modeling of functional MRI data. Neurosci Res. 65:175-186.

Gautier HO, Evans KA, Volbracht K, James R, Sitnikov S, Lundgaard I, James F, Lao-Peregrin C, Reynolds R, Franklin RJ, Karadottir RT. 2015. Neuronal activity regulates remyelination via glutamate signalling to oligodendrocyte progenitors. Nat Commun. 6:8518.

Goebel R, Esposito F, Formisano E. 2006. Analysis of functional image analysis contest (FIAC) data with brainvoyager QX: From single-subject to cortically aligned group general linear model analysis and self-organizing group independent component analysis. Hum Brain Mapp. 27:392-401.

Heine L, Bahri MA, Cavaliere C, Soddu A, Laureys S, Ptito M, Kupers R. 2015. Prevalence of increases in functional connectivity in visual, somatosensory and language areas in congenital blindness. Front Neuroanat. 9:86.

Hill RA, Patel KD, Goncalves CM, Grutzendler J, Nishiyama A. 2014. Modulation of oligodendrocyte generation during a critical temporal window after NG2 cell division. Nat Neurosci. 17:1518-1527.

Ishibashi T, Dakin KA, Stevens B, Lee PR, Kozlov SV, Stewart CL, Fields RD. 2006. Astrocytes promote myelination in response to electrical impulses. Neuron. 49:823-832.

Jiang J, Zhu W, Shi F, Liu Y, Li J, Qin W, Li K, Yu C, Jiang T. 2009. Thick visual cortex in the early blind. J Neurosci. 29:2205-2211.

Johnson JA, Zatorre RJ. 2005. Attention to simultaneous unrelated auditory and visual events: behavioral and neural correlates. Cereb Cortex. 15:1609-1620.

Johnson JA, Zatorre RJ. 2006. Neural substrates for dividing and focusing attention between simultaneous auditory and visual events. Neuroimage. 31:1673-1681.

Kawashima R, Imaizumi S, Mori K, Okada K, Goto R, Kiritani S, Ogawa A, Fukuda H. 1999. Selective visual and auditory attention toward utterances-a PET study. Neuroimage. 10:209-215.

Kennedy KM, Raz N. 2009. Aging white matter and cognition: differential effects of regional variations in diffusion properties on memory, executive functions, and speed. Neuropsychologia. 47:916-927.

Klinge C, Eippert F, Roder B, Buchel C. 2010. Corticocortical connections mediate primary visual cortex responses to auditory stimulation in the blind. J Neurosci. 30:12798-12805.

Kolasinski J, Stagg CJ, Chance SA, Deluca GC, Esiri MM, Chang EH, Palace JA, McNab JA, Jenkinson M, Miller KL, Johansen-Berg H. 2012. A combined post-mortem magnetic resonance imaging and quantitative histological study of multiple sclerosis pathology. Brain. 135:2938-2951.

Lao Y, Kang Y, Collignon O, Brun C, Kheibai SB, Alary F, Gee J, Nelson MD, Lepore F, Lepore N. 2015. A study of brain white matter plasticity in early blinds using tract-based spatial statistics and tract statistical analysis. Neuroreport. 26:1151-1154.

Laurienti PJ, Burdette JH, Wallace MT, Yen YF, Field AS, Stein BE. 2002. Deactivation of sensory-specific cortex by cross-modal stimuli. J Cogn Neurosci. 14:420-429.

Le Bihan D. 2006. Looking into the functional architecture of the brain with diffusion MRI. International Congress Series. 1290:1 – 24.

Lee VK, Nau AC, Laymon C, Chan KC, Rosario BL, Fisher C. 2014. Successful tactile based visual sensory substitution use functions independently of visual pathway integrity. Front Hum Neurosci. 8:291.

Lepore N, Voss P, Lepore F, Chou YY, Fortin M, Gougoux F, Lee AD, Brun C, Lassonde M, Madsen SK, Toga AW, Thompson PM. 2010. Brain structure changes visualized in early- and late-onset blind subjects. Neuroimage. 49:134-140.

Liu Y, Yu C, Liang M, Li J, Tian L, Zhou Y, Qin W, Li K, Jiang T. 2007. Whole brain functional connectivity in the early blind. Brain. 130:2085-2096.

Lovden M, Bodammer NC, Kuhn S, Kaufmann J, Schutze H, Tempelmann C, Heinze HJ, Duzel E, Schmiedek F, Lindenberger U. 2010. Experience-dependent plasticity of white-matter microstructure extends into old age. Neuropsychologia. 48:3878-3883.

Mackey AP, Whitaker KJ, Bunge SA. 2012. Experience-dependent plasticity in white matter microstructure: reasoning training alters structural connectivity. Front Neuroanat. 6:32.

Mamah D, Conturo TE, Harms MP, Akbudak E, Wang L, McMichael AR, Gado MH, Barch DM, Csernansky JG. 2010. Anterior thalamic radiation integrity in schizophrenia: a diffusion-tensor imaging study. Psychiatry Res. 183:144-150.

Mars RB, Foxley S, Verhagen L, Jbabdi S, Sallet J, Noonan MP, Neubert FX, Andersson JL, Croxson PL, Dunbar RI, Khrapitchev AA, Sibson NR, Miller KL, Rushworth MF. 2016. The extreme capsule fiber complex in humans and macaque monkeys: a comparative diffusion MRI tractography study. Brain Struct Funct. 221:4059-4071.

Miller LM, Recanzone GH. 2009. Populations of auditory cortical neurons can accurately encode acoustic space across stimulus intensity. Proc Natl Acad Sci U S A. 106:5931-5935.

Mori S, Zhang J. 2006. Principles of diffusion tensor imaging and its applications to basic neuroscience research. Neuron. 51:527-539.

Mozolic JL, Joyner D, Hugenschmidt CE, Peiffer AM, Kraft RA, Maldjian JA, Laurienti PJ. 2008. Cross-modal deactivations during modality-specific selective attention. BMC Neurol. 8:35.

Murray MM, Thelen A, Thut G, Romei V, Martuzzi R, Matusz PJ. 2016. The multisensory function of the human primary visual cortex. Neuropsychologia. 83:161-169.

Nagy Z, Westerberg H, Klingberg T. 2004. Maturation of white matter is associated with the development of cognitive functions during childhood. J Cogn Neurosci. 16:1227-1233.

Noppeney U, Friston KJ, Ashburner J, Frackowiak R, Price CJ. 2005. Early visual deprivation induces structural plasticity in gray and white matter. Curr Biol. 15:R488-490.

Olesen PJ, Nagy Z, Westerberg H, Klingberg T. 2003. Combined analysis of DTI and fMRI data reveals a joint maturation of white and grey matter in a fronto-parietal network. Brain Res Cogn Brain Res. 18:48-57.

Onu M, Roceanu A, Sboto-Frankenstein U, Bendic R, Tarta E, Preoteasa F, Bajenaru O. 2012. Diffusion abnormality maps in demyelinating disease: correlations with clinical scores. Eur J Radiol. 81:e386-391.

Pan WJ, Wu G, Li CX, Lin F, Sun J, Lei H. 2007. Progressive atrophy in the optic pathway and visual cortex of early blind Chinese adults: A voxel-based morphometry magnetic resonance imaging study. Neuroimage. 37:212-220.

Park HJ, Jeong SO, Kim EY, Kim JI, Park H, Oh MK, Kim DJ, Kim SY, Lee SC, Lee JD. 2007. Reorganization of neural circuits in the blind on diffusion direction analysis. Neuroreport. 18:1757-1760.

Park HJ, Lee JD, Kim EY, Park B, Oh MK, Lee S, Kim JJ. 2009. Morphological alterations in the congenital blind based on the analysis of cortical thickness and surface area. Neuroimage. 47:98-106.

Pelland M, Orban P, Dansereau C, Lepore F, Bellec P, Collignon O. 2017. State-dependent modulation of functional connectivity in early blind individuals. Neuroimage. 147:532-541.

Ptito M, Schneider FC, Paulson OB, Kupers R. 2008. Alterations of the visual pathways in congenital blindness. Exp Brain Res. 187:41-49.

Rauschecker JP, Tian B. 2000. Mechanisms and streams for processing of "what" and "where" in auditory cortex. Proc Natl Acad Sci U S A. 97:11800-11806.

Rea P. 2015. Essential Clinical Anatomy of the Nervous System. London: Academic Press.

Recanzone GH. 2000. Spatial processing in the auditory cortex of the macaque monkey. Proc Natl Acad Sci U S A. 97:11829-11835.

Reislev NL, Dyrby TB, Siebner HR, Kupers R, Ptito M. 2016a. Simultaneous Assessment of White Matter Changes in Microstructure and Connectedness in the Blind Brain. Neural Plast. 2016:6029241.

Reislev NL, Kupers R, Siebner HR, Ptito M, Dyrby TB. 2016b. Blindness alters the microstructure of the ventral but not the dorsal visual stream. Brain Struct Funct. 221:2891-2903.

Renier LA, Anurova I, De Volder AG, Carlson S, VanMeter J, Rauschecker JP. 2010. Preserved functional specialization for spatial processing in the middle occipital gyrus of the early blind. Neuron. 68:138-148.

Rockland KS, Ojima H. 2003. Multisensory convergence in calcarine visual areas in macaque monkey. Int J Psychophysiol. 50:19-26.

Romanski LM, Tian B, Fritz J, Mishkin M, Goldman-Rakic PS, Rauschecker JP. 1999. Dual streams of auditory afferents target multiple domains in the primate prefrontal cortex. Nat Neurosci. 2:1131-1136.

Salminen T, Martensson J, Schubert T, Kuhn S. 2016. Increased integrity of white matter pathways after dual n-back training. Neuroimage. 133:244-250.

Sampaio-Baptista C, Johansen-Berg H. 2017. White Matter Plasticity in the Adult Brain. Neuron. 96:1239-1251.

Sani L, Ricciardi E, Gentili C, Vanello N, Haxby JV, Pietrini P. 2010. Effects of Visual Experience on the Human MT+ Functional Connectivity Networks: An fMRI Study of Motion Perception in Sighted and Congenitally Blind Individuals. Front Syst Neurosci. 4:159.

Saur D, Kreher BW, Schnell S, Kummerer D, Kellmeyer P, Vry MS, Umarova R, Musso M, Glauche V, Abel S, Huber W, Rijntjes M, Hennig J, Weiller C. 2008. Ventral and dorsal pathways for language. Proc Natl Acad Sci U S A. 105:18035-18040.

Schmahmann JD, Pandya DN, Wang R, Dai G, D'Arceuil HE, de Crespigny AJ, Wedeen VJ. 2007. Association fibre pathways of the brain: parallel observations from diffusion spectrum imaging and autoradiography. Brain. 130:630-653.

Schmierer K, Wheeler-Kingshott CA, Boulby PA, Scaravilli F, Altmann DR, Barker GJ, Tofts PS, Miller DH. 2007. Diffusion tensor imaging of post mortem multiple sclerosis brain. Neuroimage. 35:467-477.

Shimony JS, Burton H, Epstein AA, McLaren DG, Sun SW, Snyder AZ. 2006. Diffusion tensor imaging reveals white matter reorganization in early blind humans. Cereb Cortex. 16:1653-1661.

Shomstein S, Yantis S. 2004. Control of attention shifts between vision and audition in human cortex. J Neurosci. 24:10702-10706.

Shu N, Li J, Li K, Yu C, Jiang T. 2009a. Abnormal diffusion of cerebral white matter in early blindness. Hum Brain Mapp. 30:220-227.

Shu N, Liu Y, Li J, Li Y, Yu C, Jiang T. 2009b. Altered anatomical network in early blindness revealed by diffusion tensor tractography. PLoS One. 4:e7228.

Smith SM. 2002. Fast robust automated brain extraction. Hum Brain Mapp. 17:143-155.

Smith SM, Jenkinson M, Johansen-Berg H, Rueckert D, Nichols TE, Mackay CE, Watkins KE, Ciccarelli O, Cader MZ, Matthews PM, Behrens TE. 2006. Tract-based spatial statistics: voxelwise analysis of multi-subject diffusion data. Neuroimage. 31:1487-1505.

Smith SM, Jenkinson M, Woolrich MW, Beckmann CF, Behrens TE, Johansen-Berg H, Bannister PR, De Luca M, Drobnjak I, Flitney DE, Niazy RK, Saunders J, Vickers J, Zhang Y, De Stefano N, Brady JM, Matthews PM. 2004. Advances in functional and structural MR image analysis and implementation as FSL. Neuroimage. 23 Suppl 1:S208-219.

Song SK, Sun SW, Ramsbottom MJ, Chang C, Russell J, Cross AH. 2002. Dysmyelination revealed through MRI as increased radial (but unchanged axial) diffusion of water. Neuroimage. 17:1429-1436.

Song SK, Yoshino J, Le TQ, Lin SJ, Sun SW, Cross AH, Armstrong RC. 2005. Demyelination increases radial diffusivity in corpus callosum of mouse brain. Neuroimage. 26:132-140.

Spierer L, Bellmann-Thiran A, Maeder P, Murray MM, Clarke S. 2009. Hemispheric competence for auditory spatial representation. Brain. 132:1953-1966.

Stevens B, Porta S, Haak LL, Gallo V, Fields RD. 2002. Adenosine: a neuron-glial transmitter promoting myelination in the CNS in response to action potentials. Neuron. 36:855-868.

Stilla R, Hanna R, Hu X, Mariola E, Deshpande G, Sathian K. 2008. Neural processing underlying tactile microspatial discrimination in the blind: a functional magnetic resonance imaging study. J Vis. 8:13 11-19.

Striem-Amit E, Ovadia-Caro S, Caramazza A, Margulies DS, Villringer A, Amedi A. 2015. Functional connectivity of visual cortex in the blind follows retinotopic organization principles. Brain. 138:1679-1695.

Sun SW, Liang HF, Cross AH, Song SK. 2008. Evolving Wallerian degeneration after transient retinal ischemia in mice characterized by diffusion tensor imaging. Neuroimage. 40:1-10.

Takemura H, Pestilli F, Weiner KS, Keliris GA, Landi SM, Sliwa J, Ye FQ, Barnett MA, Leopold DA, Freiwald WA, Logothetis NK, Wandell BA. 2017. Occipital White Matter Tracts in Human and Macaque. Cereb Cortex. 27:3346-3359.

Takeuchi H, Sekiguchi A, Taki Y, Yokoyama S, Yomogida Y, Komuro N, Yamanouchi T, Suzuki S, Kawashima R. 2010. Training of working memory impacts structural connectivity. J Neurosci. 30:3297-3303.

Talairach G, Tournoux P. 1988. Co-Planar Stereotaxic Atlas of the Human Brain. New York: Thieme.

Tian B, Reser D, Durham A, Kustov A, Rauschecker JP. 2001. Functional specialization in rhesus monkey auditory cortex. Science. 292:290-293.

Voss P, Zatorre RJ. 2012. Occipital cortical thickness predicts performance on pitch and musical tasks in blind individuals. Cereb Cortex. 22:2455-2465.

Wake H, Ortiz FC, Woo DH, Lee PR, Angulo MC, Fields RD. 2015. Nonsynaptic junctions on myelinating glia promote preferential myelination of electrically active axons. Nat Commun. 6:7844.

Wang D, Qin W, Liu Y, Zhang Y, Jiang T, Yu C. 2013. Altered white matter integrity in the congenital and late blind people. Neural Plast. 2013:128236.

Wang D, Qin W, Liu Y, Zhang Y, Tianzi J, Yu C. 2014. Altered resting-state network connectivity in congenital blind. Human Brain Mapp. 35:2573-2581.

Warren JD, Griffiths TD. 2003. Distinct mechanisms for processing spatial sequences and pitch sequences in the human auditory brain. J Neurosci. 23:5799-5804.

Watson JD, Myers R, Frackowiak RS, Hajnal JV, Woods RP, Mazziotta JC, Shipp S, Zeki S. 1993. Area V5 of the human brain: evidence from a combined study using positron emission tomography and magnetic resonance imaging. Cereb Cortex. 3:79-94.

Weeks R, Horwitz B, Aziz-Sultan A, Tian B, Wessinger CM, Cohen LG, Hallett M, Rauschecker JP. 2000. A positron emission tomographic study of auditory localization in the congenitally blind. J Neurosci. 20:2664-2672.

Weisz N, Muller N, Jatzev S, Bertrand O. 2014. Oscillatory alpha modulations in right auditory regions reflect the validity of acoustic cues in an auditory spatial attention task. Cereb Cortex. 24:2579-2590.

Yu C, Liu Y, Li J, Zhou Y, Wang K, Tian L, Qin W, Jiang T, Li K. 2008. Altered functional connectivity of primary visual cortex in early blindness. Hum Brain Mapp. 29:533-543.

Yu C, Shu N, Li J, Qin W, Jiang T, Li K. 2007. Plasticity of the corticospinal tract in early blindness revealed by quantitative analysis of fractional anisotropy based on diffusion tensor tractography. Neuroimage. 36:411-417.

Zahr NM, Rohlfing T, Pfefferbaum A, Sullivan EV. 2009. Problem solving, working memory, and motor correlates of association and commissural fiber bundles in normal aging: a quantitative fiber tracking study. Neuroimage. 44:1050-1062.

Zatorre RJ, Penhune VB. 2001. Spatial localization after excision of human auditory cortex. J Neurosci. 21:6321-6328.

Zhang Y, Wan S, Ge J, Zhang X. 2012. Diffusion tensor imaging reveals normal geniculocalcarine-tract integrity in acquired blindness. Brain Res. 1458:34-39.

Table 1. Clinical characteristics of EB subjects

Subject	Sex	Age (years)	Cause of blindness	Onset of blindness	Light perception
EB01	Male	56	ROP	Congenital	NLP
EB02	Male	45	Retinopathy	< 2 years	NLP
EB03	Female	56	Unknown	Congenital	Yes (right eye)
EB04	Male	38	Detached retinas	< 2 years	NLP
EB05	Female	58	ROP	Congenital	Yes
EB06	Female	64	Congenital glaucoma	Congenital	NLP
EB07	Male	53	ROP	Congenital	Yes
EB08	Male	55	Retinal detachment	Congenital	Yes (right eye)
EB09	Female	34	Optic nerve hypoplasia	< 2 years	Yes
EB10	Female	34	ROP	Congenital	NLP
EB11	Female	55	ROP	Congenital	Yes (right eye)
EB12	Male	61	Unknown	Congenital	NLP
EB13	Female	55	ROP	Congenital	NLP
EB14	Male	56	ROP	Congenital	NLP
EB15	Female	56	ROP	Congenital	NLP

ROP = retinopathy of prematurity; NLP = no light perception

Figure captions

Fig. 1. Differences in (A) fractional anisotropy (FA) and (B) axial diffusivity (AD) between the groups of early blind and sighted controls revealed by TBSS. Dark gray color represents the mean FA skeleton of all participants. Red-yellow colors represent significant decreases and blue-lightblue colors represent significant increases in the DTI measures of EB compared to SC ($p < 0.05$ after threshold-free cluster enhancement (TFCE) correction; data are controlled for age and gender). White arrows indicate white-matter tracts where significant differences between groups were observed. GCT – geniculo-calcarine tract; IFOF – inferior fronto-occipital fasciculus; ATR – anterior thalamic radiation; ILF – inferior longitudinal fasciculus; aCC and pCC – anterior and posterior parts of corpus callosum; CST – corticospinal tract; LH and RH – left and right hemisphere. The images are displayed in radiological convention with right hemisphere shown on the left side.

Fig. 2. Differences in (A) radial (RD) and (B) mean diffusivity (MD) between the groups of early blind and sighted controls revealed by TBSS. Dark gray color represents the mean FA skeleton of all participants. Blue-light blue colors represent increases in the DTI measures of EB compared to SC ($p < 0.05$ after TFCE correction; data are controlled for age and gender). All other designations and abbreviations as in Fig. 1.

Fig. 3. Relationship between FA and behavioral performance. A. White-matter regions where significant correlations between FA and accuracy of LOC task performance were observed are shown using red-yellow colors ($p < 0.05$ after TFCE correction; data are controlled for age and gender). B. Scatter plots depict dependence of LOC task performance accuracy on FA within the significant cluster (A) in the groups of EB (red dots) and SC (blue dots). r_p – partial correlation coefficient, ** = $p < 0.01$, *** = $p < 0.001$. C. Results of probabilistic tractography using the significant cluster (A) as a seed. Group-averaged tracts for EB participants are shown in red-yellow, for SC in blue-light blue. The tracts are normalized and

thresholded at 0.02%. D. Examples of individual tracts in one EB (red-yellow) and one SC participant (blue-light blue). The tracts connect right-hemispheric STG with medial and lateral occipital areas.

Fig. 4. A. Regions of interest depicted from fMRI data. CS – calcarine sulcus, LO – lateral occipital cortex, STG – superior temporal gyrus, LH – left hemisphere, RH – right hemisphere. B – D. Relationship between FA and right STG ROI activation during ID task performance. B. White-matter regions where significant correlations between the FA and activation were observed are shown using red-yellow colors ($p < 0.05$ after TFCE correction; data are controlled for age and gender). C. Scatter plots depict dependence of the right STG activation in ID task on FA within the significant cluster (A) in the groups of EB (red dots) and SC (blue dots). D. Group-averaged tracts passing through the significant cluster (A) in EB (red-yellow) and SC (blue-light blue). The tracts are normalized and thresholded at 0.02%. Frontal transcallosal (bottom row, left), thalamo-cortical (upper row) connections and left IFOF (bottom row, middle and right) are observed. All other designations as in Figs. 1 and 3.

Fig. 5. Relationship between FA and right STG ROI activation during LOC task performance (A – C) and between FA and left STG ROI activation during LOC task performance (D – F). A and D. White-matter regions where significant correlations between the FA and activation were observed are shown using red-yellow colors ($p < 0.05$ after TFCE correction; data are controlled for age and gender). B and E. Scatter plots depict dependence of the right (B) and left (E) STG activation by LOC task on FA within the significant clusters in the groups of EB (red dots) and SC (blue dots). C and F. Group-averaged tracts passing through the significant clusters in EB (red-yellow) and SC (blue-light blue). The tracts are normalized and thresholded at 0.02%. Frontal transcallosal (C and F, bottom rows, left), thalamo-cortical (C and F, upper rows) connections, left IFOF (C and F, bottom rows, middle and right) and left SLF (C, bottom row, right) are observed. All other designations as in Figs. 1 and 3.

Fig. 6. Relationship between FA and right CS ROI activation during ID task performance (A – C) and between FA and right LO ROI activation during LOC task performance (D – F). A and D. White-matter regions where significant interactions between effects of Group and Activation were observed are shown using red-yellow colors ($p < 0.05$ after TFCE correction; data are controlled for age and gender). B and E. Scatter plots depict dependence of the right CS activation by ID task (B) and the right LO activation by LOC task (E) on FA within the significant clusters in the groups of EB (red dots) and SC (blue dots). C and F. Group-averaged tracts passing through the significant clusters in EB (red-yellow) and SC (blue-light blue). The tracts are normalized and thresholded at 0.02%. Frontal transcallosal (C and F, bottom rows, left), thalamo-cortical (C and F, upper rows) connections and bilateral (C) and left (F) IFOF (bottom rows, middle and right) are observed. All other designations as in Figs. 1 and 3.

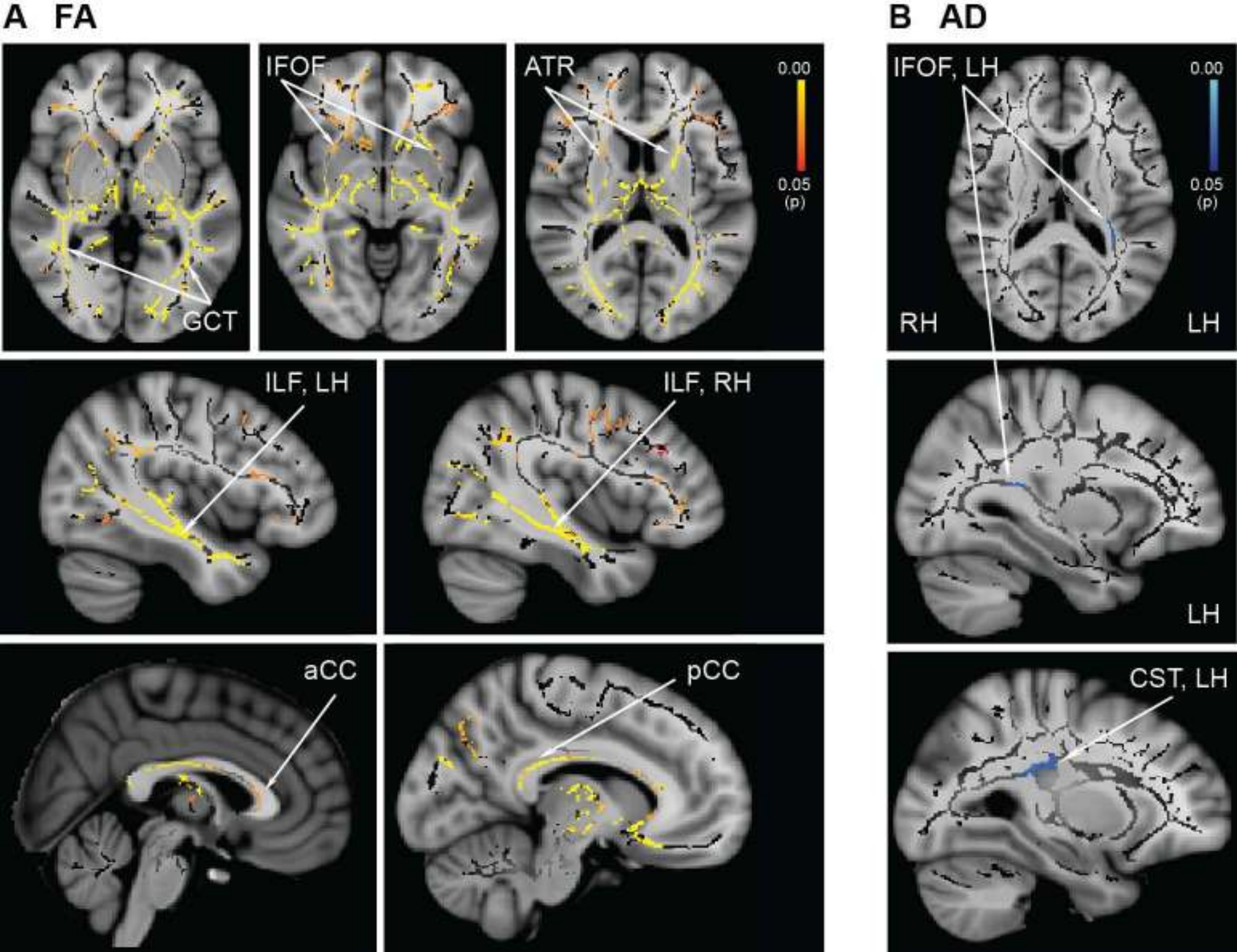
A FA
IFOF
ATR
0.00
0.05
(p)
GCT
ILF, LH
ILF, RH
aCC
pCC
B AD
IFOF, LH
0.00
0.05
(p)
RH
LH
LH
CST, LH

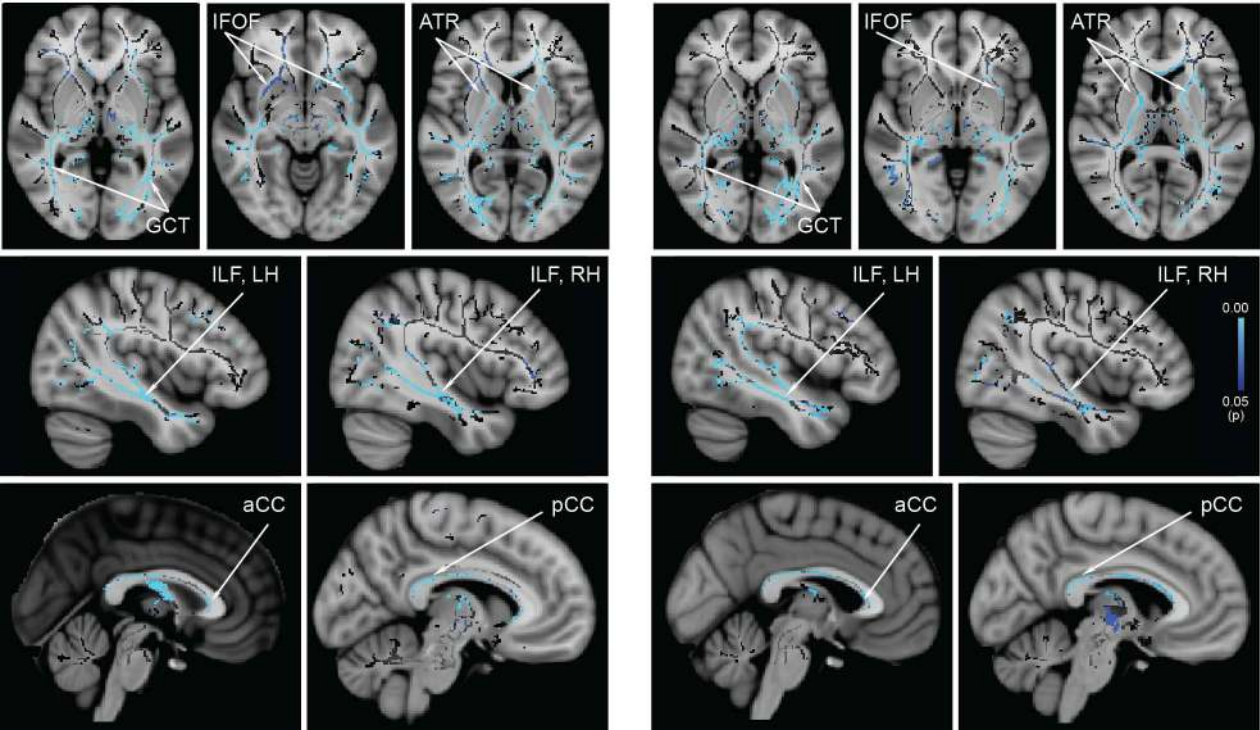
A RD
IFOF
ATR
GCT
ILF, LH
ILF, RH
aCC
pCC
B MD
IFOF
ATR
GCT
ILF, LH
ILF, RH
0.00
0.05
(p)
aCC
pCC

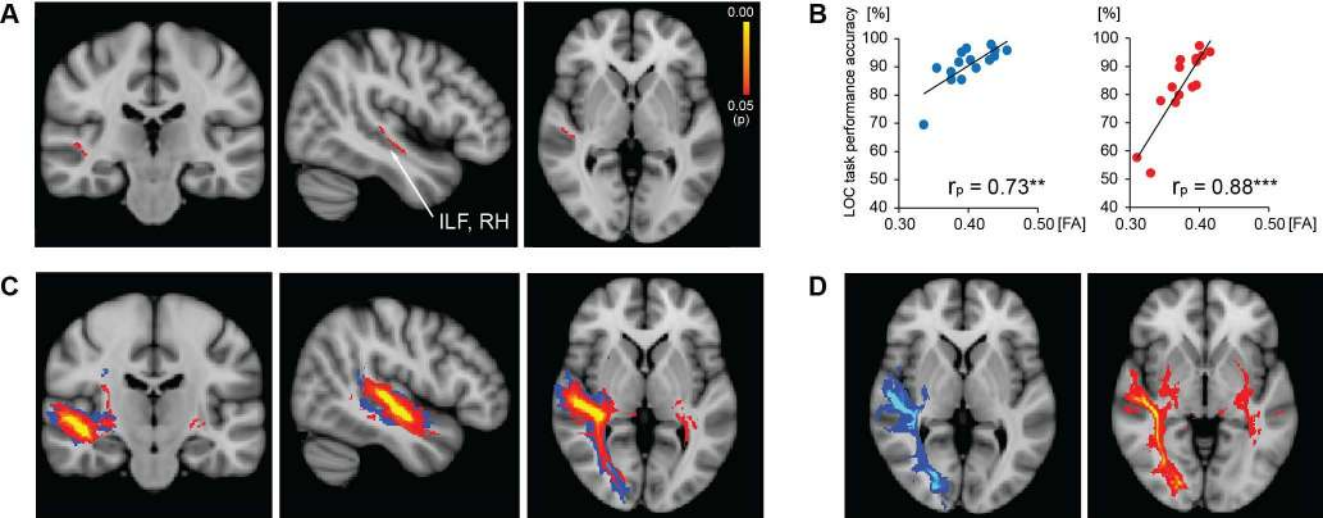
A
0.00
0.05
(p)
ILF, RH
B
[%]
LOC task performance accuracy
100
90
80
70
60
50
40
0.30
0.40
0.50 [FA]
r_p = 0.73**
[%]
100
90
80
70
60
50
40
0.30
0.40
0.50 [FA]
r_p = 0.88***
C
D

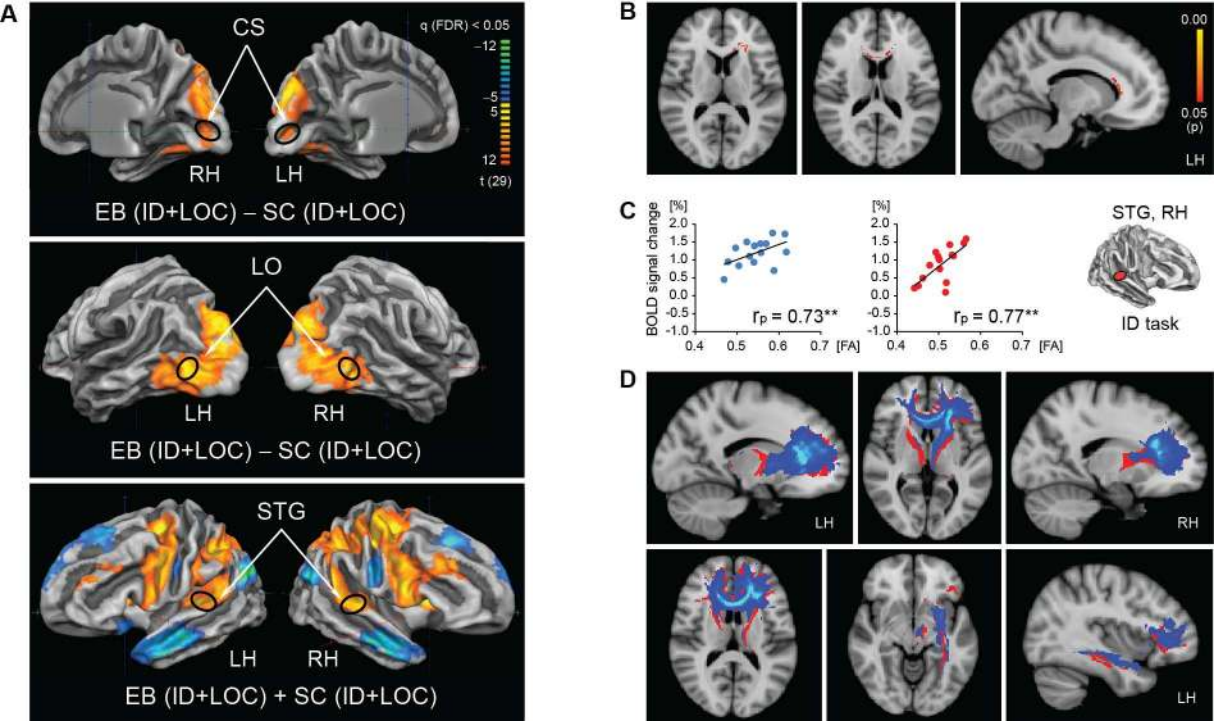
A
CS
q (FDR) < 0.05
−12
−5
5
12
t (29)
RH
LH
EB (ID+LOC) – SC (ID+LOC)
LO
LH
RH
EB (ID+LOC) – SC (ID+LOC)
STG
LH
RH
EB (ID+LOC) + SC (ID+LOC)
B
0.00
0.05
(p)
LH
C
BOLD signal change
[%]
2.0
1.5
1.0
0.5
0.0
−0.5
−1.0
0.4
0.5
0.6
0.7
[FA]
rp = 0.73**
rp = 0.77**
STG, RH
ID task
D
LH
RH
LH

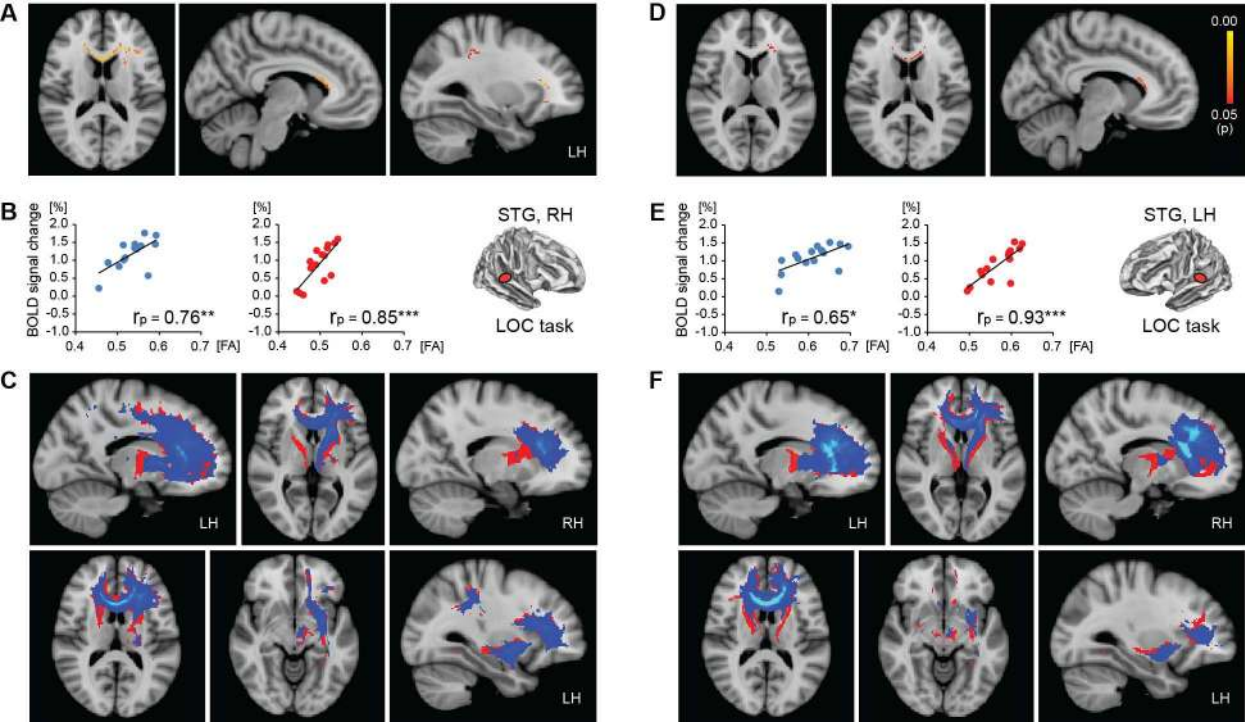
A
LH
D
0.00
0.05
(p)
B
[%]
BOLD signal change
2.0
1.5
1.0
0.5
0.0
-0.5
-1.0
0.4
0.5
0.6
0.7 [FA]
rp = 0.76**
rp = 0.85***
STG, RH
LOC task
E
rp = 0.65*
rp = 0.93***
STG, LH
LOC task
C
LH
RH
F

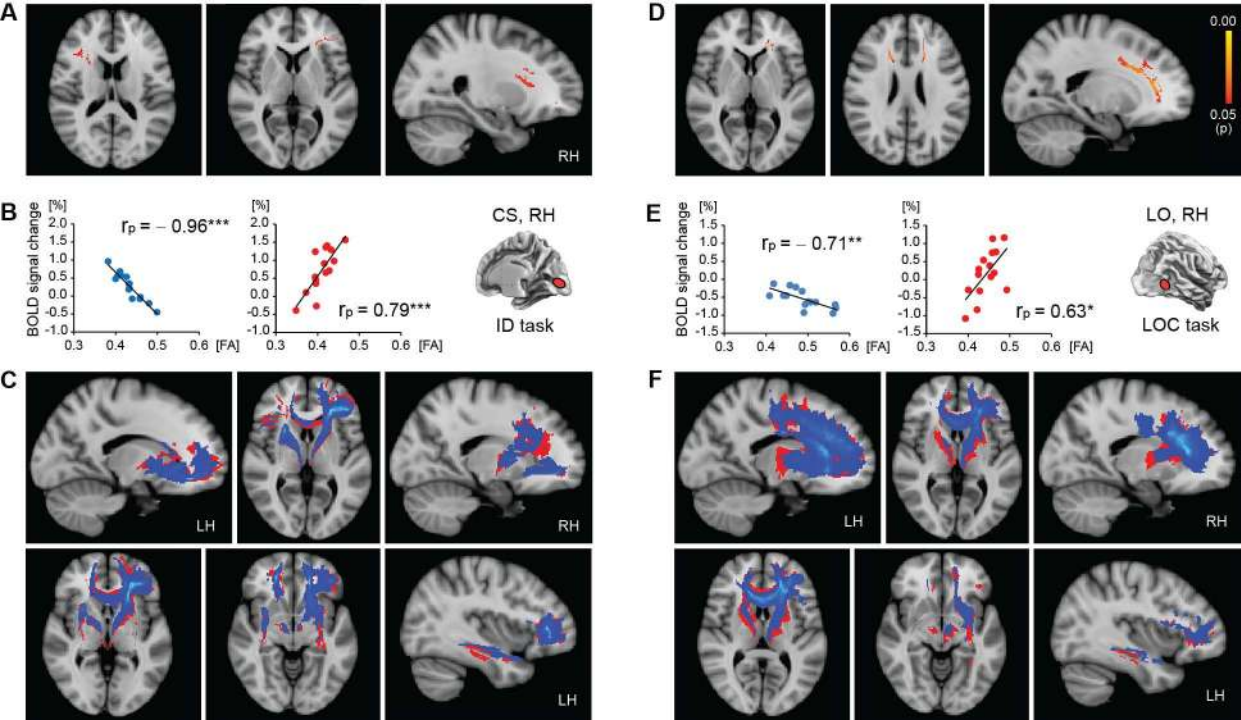
A
RH
D
0.00
0.05
(p)
B
[%]
BOLD signal change
$r_p = -0.96^{***}$
[FA]
$r_p = 0.79^{***}$
CS, RH
ID task
E
$r_p = -0.71^{**}$
$r_p = 0.63^{*}$
LO, RH
LOC task
C
LH
RH
F